

The AbinitioDΓA Project v1.0: Non-local correlations beyond and susceptibilities within dynamical mean-field theory

Anna Galler^{a,b,*}, Patrik Thunström^{a,c}, Josef Kaufmann^a, Matthias Pickem^a, Jan M. Tomczak^a, Karsten Held^a

^a*Institute of Solid State Physics, TU Wien, 1040 Vienna, Austria*

^b*Centre de Physique Théorique, Ecole Polytechnique, 91128 Palaiseau, France*

^c*Department of Physics and Astronomy, Materials Theory, Uppsala University, 75120 Uppsala, Sweden*

Abstract

The *ab initio* extension of the dynamical vertex approximation (DΓA) method allows for realistic materials calculations that include non-local correlations beyond *GW* and dynamical mean-field theory. Here, we discuss the AbinitioDΓA algorithm, its implementation and usage in detail, and make the program package available to the scientific community.

Keywords: Strongly correlated electron systems; dynamical mean-field theory; dynamical vertex approximation; electronic structure calculations

PROGRAM SUMMARY

Program Title: AbinitioDΓA

Licensing provisions: GPLv3

Programming language: Fortran 90

Supplementary material: Testcase files and step-by-step instructions

Nature of problem: Realistic materials calculations including non-local correlations beyond dynamical mean-field theory (DMFT) as well as non-local interactions. Solving the Bethe-Salpeter equation for multiple orbitals. Determining momentum-resolved susceptibilities in DMFT.

Solution method:

Ab initio dynamical vertex approximation: starting from the local two-particle vertex and constructing from it the local DMFT correlations, the *GW* diagrams, and further non-local correlations, e.g., spin fluctuations. Efficient solution of the Bethe-Salpeter equation, avoiding divergencies in the irreducible vertex in the particle-hole channel by reformulating the problem in terms of the full vertex. Parallelization with respect to the bosonic frequency and momentum.

Additional comments including Restrictions and Unusual features:

As input, a Hamiltonian derived, e.g., from density functional theory and a DMFT solution thereof is needed including a local two-particle vertex calculated at DMFT self-consistency. Hitherto the AbinitioDΓA program package is restricted to $SU(2)$ symmetric problems. A so-called λ correction or self-consistency is not yet implemented in the AbinitioDΓA code. Susceptibilities are so far only calculated within DMFT not the dynamical vertex approximation.

1. Introduction

Dynamical mean-field theory (DMFT) [1, 2] takes into account a major part of the electronic correlations, namely the local ones. It has been very successfully applied to models of strongly correlated electron system, see [3] for an early review and [4] for a series of lecture notes on the occasion of 25 years of DMFT. Its merger with density functional theory (DFT) [5, 6] and *GW* [7, 8] even allows for the realistic calculation of materials including strong electronic correlations, see [9, 10] and [11] for reviews.

On the other hand, non-local correlations are at the heart of many fascinating phenomena of many-body physics. In the aforementioned *GW*+DMFT approach the screening of the bare interaction V to a screened W gives rise to

*Corresponding author.

E-mail address: galler.anna@gmail.com

non-local correlations in the self-energy. But there are important further effects of non-local correlations, e.g., spin fluctuations. Hence, extensions of DMFT that include the local DMFT correlations and additional non-local correlations are at the scientific frontier.

One main route to this end are cluster extensions of DMFT which consider a cluster of sites in a DMFT Weiss field. Two methods, the dynamical cluster approximation (DCA) [12] and the cellular DMFT [13, 14], have been developed, see [15] for a review. Due to numerical limitations these approaches are restricted to short-range correlations and essentially a single interacting band. Realistic calculations are hardly possible or restricted to extremely small clusters [16, 17].

Diagrammatic extensions of the DMFT on the other hand use a local two-particle vertex as a starting point and construct from it the local DMFT correlations as well as non-local correlations. These diagrammatic extensions are more suitable to deal with long-range correlations and realistic multi-orbital calculations. This more recent development started with the dynamical vertex approximation (D Γ A) [18, 19], subsequently followed by various other approaches such as the dual fermion approach [20], the one-particle irreducible (1PI) approach [21], the dynamical mean-field theory to functional renormalization group (DMF²RG) approach [22], the triply-irreducible local expansion (TRILEX) [23] and the non-local expansion scheme [24]. These diagrammatic extensions of DMFT have been first applied to model systems, among others to calculate (quantum) critical exponents [25, 26, 27, 28], see [29] for a review.

Most recently, these diagrammatic approaches have been extended to realistic multi-orbital *ab initio* D Γ A calculations [30, 31]. Using the local three-frequency and four-orbital vertex and on top of this the non-local bare interaction as a starting point, this approach not only includes the DMFT and *GW* Feynman diagrams but also many further non-local correlations. It is the aim of this paper to make the developed AbinitioD Γ A program package available to the general scientific community.

The paper is organized as follows: In Section 2, we recapitulate the AbinitioD Γ A formalism of [30] and how the program calculates (non-local) self-energies (Section 2.1) and susceptibilities (Section 2.2). Section 3 provides an overview of the program structure. The starting point of the calculation is a DFT+DMFT calculation where after convergence the two-particle Green's function is calculated, as explained in Section 3.1. From this the two-particle vertex is obtained, as outlined in Section 3.2, possibly including symmetry operations to improve the statistics. In Section 3.3 we turn to the actual program structure of the main AbinitioD Γ A program, including a discussion of algorithmic details in Section 4, the storage of the two-particle Green's functions in hdf5 file format in Section 4.1, and the compound orbital-frequency index for matrix operations in Section 4.2. Information regarding the numerical effort for calculating the vertex and from it the AbinitioD Γ A self-energy is provided in Section 4.3. In Section 5 we show some exemplary results for the DMFT susceptibility and AbinitioD Γ A self-energy for the compound SrVO₃. Finally, Section 6 provides a conclusion and outlook.

2. Implemented AbinitioD Γ A equations

2.1. AbinitioD Γ A self-energy

The main quantity, which is computed by the AbinitioD Γ A algorithm, is the non-local (\mathbf{k} -dependent) and dynamical (ν -dependent) self-energy $\Sigma_{\text{D}\Gamma\text{A}}$. We compute $\Sigma_{\text{D}\Gamma\text{A}}$ in the ladder approximation of D Γ A [32, 33] which incorporates non-local ladder diagrams in, both, the particle-hole (ph) and transverse particle-hole (\overline{ph}) channel starting from a local irreducible vertex in these channels. This way, among others, spin fluctuations are included, but one neglects the particle-particle (pp) channel which is, e.g., important for superconducting fluctuations.

In AbinitioD Γ A the local irreducible vertex in the ph and \overline{ph} channel is supplemented by the bare non-local Coulomb interaction $V^{\mathbf{q}}$. This includes various extra diagrams and screening effects. For example, if we only have the ph channel and the non-local Coulomb interaction, one would reproduce the *GW* approximation [34]. Using the compound indices $\mathbf{k} = (\mathbf{k}, \nu)$ and $\mathbf{q} = (\mathbf{q}, \omega)$ the self-energy of the AbinitioD Γ A reads [30]

$$\begin{aligned} \Sigma_{\text{D}\Gamma\text{A}}^{\mathbf{k}} = & \Sigma_{\text{DMFT}}^{\nu} + \Sigma_{\text{HF}}^{\mathbf{k}} - \beta^{-1} \sum_{lnhh'q} \left(U_{mlhn} + V_{mlhn}^{\mathbf{q}} - \frac{1}{2} \tilde{U}_{mlnh} \right) \eta_{d,nlh'm'}^{\text{qv}} G_{hh'}^{\mathbf{k}-\mathbf{q}} \\ & + \beta^{-1} \sum_{lnhh'q} \frac{3}{2} \tilde{U}_{mlnh} \eta_{m,nlh'm'}^{\text{qv}} G_{hh'}^{\mathbf{k}-\mathbf{q}} - \beta^{-1} \sum_{lnhh'q} \left(V_{mlhn}^{\mathbf{q}} \gamma_{d,nlh'm'}^{\omega\nu} - U_{mlhn} \gamma_{d,nlh'm'}^{\text{qv}} \right) G_{hh'}^{\mathbf{k}-\mathbf{q}}. \end{aligned} \quad (1)$$

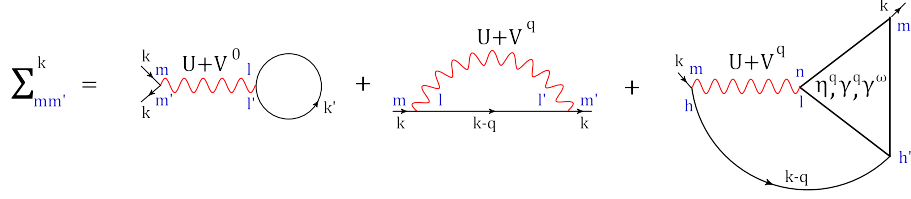


Figure 1: Feynman-diagrammatic representation of the AbinitioDFA equation of motion [Eq. (1)]: The self-energy is obtained from the three-leg vertices η^q , γ^q and γ^ω , which in turn are obtained from the full vertex F (see Fig. 3 below) that is determined via the Bethe-Salpeter equation. In addition, the Hartree and Fock contributions of Eq. (6) need to be added. Beside the momenta qk' , orbital indices $lmm'l'$ are shown in blue.

This expression for the AbinitioDFA self-energy is depicted diagrammatically in Fig. 1. In the following we will introduce all quantities necessary for the evaluation of Σ_{DFA} in Eq. (1) and discuss how these are calculated. In particular, the non-local three-leg vertices γ^{qv} and η^{qv} are obtained in DFA from the local irreducible vertex through the Bethe-Salpeter ladder. A detailed derivation can be found in Ref. [30], while further algorithmic details, e.g., how frequency- and orbital summations can be cast into an efficient matrix form, will be given in Section 4.

One-particle Green's function. The one-particle Green's function G^{k-q} appearing in the last three terms in Eq. (1) is the lattice Green's function, given by

$$G_{hh'}^k = [i\nu + \mu - H_W^k - \Sigma^\nu - \Sigma_{DC}]_{hh'}^{-1}. \quad (2)$$

Here, H_W^k is the material-dependent Hamiltonian obtained, e.g., from a DFT computation and a consecutive Wannier projection [35], Σ^ν is the dynamical but local DMFT self-energy, Σ_{DC} the double-counting correction, and μ the chemical potential of the DMFT calculation. Here, and in the following, Roman subscripts denote orbital indices, $\nu = (2n+1)\pi/\beta$ ($\omega = 2n\pi/\beta$) are fermionic (bosonic) Matsubara frequencies for an inverse temperature $\beta = 1/(k_B T)$.

From the products of two interacting one-particle Green's functions the unconnected (bare bubble) susceptibilities χ_0^ω , χ_0^q and $\chi_0^{nl,q}$ are obtained. In order of increasing non-local character, the following susceptibilities are needed:

$$\chi_{0,lmml'}^{\omega\nu\nu} = -\beta G_{ll'}^\nu G_{m'm}^{\nu-\omega}, \quad (3)$$

$$\chi_{0,lmml'}^{qv\nu} = -\beta \sum_{\mathbf{k}} G_{ll'}^k G_{m'm}^{k-q}, \quad (4)$$

$$\chi_{0,lmml'}^{nl,q\nu\nu} = \chi_{0,lmml'}^{qv\nu} - \chi_{0,lmml'}^{\omega\nu\nu}. \quad (5)$$

Here, $\chi_0^{\omega\nu\nu}$ is a purely local bubble-term obtained by the product of two local one-particle DMFT Green's functions $G_{hh'}^\nu = \sum_{\mathbf{k}} G_{hh'}^k$; $\chi_0^{qv\nu}$ instead is the q -dependent product of two non-local DMFT Green's functions defined in Eq. (2). By subtracting Eq. (3) from Eq. (4) one finally obtains the purely non-local $\chi_0^{nl,q\nu\nu}$.

Local and non-local Coulomb interaction. In the Wannier basis, local and non-local Coulomb interaction are four-index objects, denoted as $U_{lm'm'l'}$ and $V_{lm'm'l'}^q$, respectively. The current implementation allows for an arbitrary orbital-dependence of the Coulomb interaction without any restriction in performance. The \tilde{U} in Eq. (1) is the local Coulomb interaction in the transverse particle-hole ($\bar{p}h$) channel and is related to U through $\tilde{U}_{lm'm'l'} = U_{lm'l'm}$. The two channels are visualized in Fig. 2 for the non-local Coulomb interaction. However, the non-local component in the $\bar{p}h$ -channel, $\tilde{V}_{lm'l'm}^{k'-k}$, is neglected in the AbinitioDFA formalism (for details see Ref. [30, 31]). This approximation is common practice: Indeed the GW approach [7, 8] neglects both local and non-local interactions in the transverse channel.

DMFT and Hartree-Fock contribution. The first contribution to Σ_{DFA}^k in Eq. (1) is the DMFT self-energy Σ_{DMFT}^ν that contains all diagrams that can be build from the local Green's function $G^\nu = \sum_{\mathbf{k}} G^k$ and the local interaction U . This contribution is the leading term to Σ_{DFA}^k at large frequencies ν . Σ_{DMFT}^ν includes the local and static Hartree-Fock term originating from the local Coulomb interaction U . However, AbinitioDFA also contains the non-local Hartree-Fock

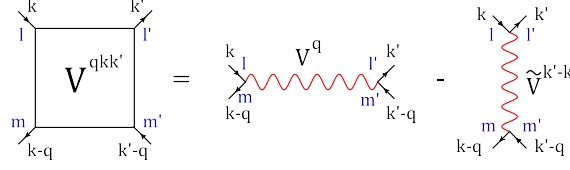


Figure 2: The non-local Coulomb interaction $V^{qkk'}$ consists of two terms: V^q and $V^{k'-k}$ (the latter is neglected in the AbinitioDGA approach). The local Coulomb interaction U has the same structure, but without any momentum dependence so that both terms can be taken into account without effort.

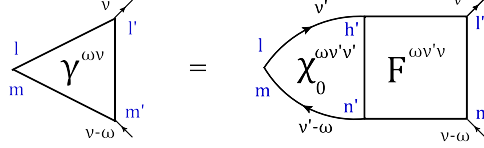


Figure 3: The three-leg vertices are obtained from $\chi_0 F$ through a sum over the left fermionic frequency v' . Here, exemplary, the relation for the purely local three-leg vertex $\gamma^{\omega v}$ in Eq. (7) is shown.

term arising from the non-local Coulomb interaction V^q . Indeed, the second term in Eq. (1), Σ_{HF}^k , is the non-local, static Hartree-Fock contribution and reads

$$\Sigma_{\text{HF}}^k = 2 \sum_{ll'k'} V^{q=0}_{mlm'l'} n_{ll'}^k - \sum_{ll'q} V^q_{ml'l'm'} n_{ll'}^{k-q}, \quad (6)$$

where $n^k = 1/\beta \sum_v G^k$ are the k -dependent occupancies.

Three-leg vertices. The quantities $\gamma_r^{\omega v}$, γ_r^{qv} and η_r^{qv} in Eq. (1) (with the index r referring to the (d)ensity or (m)agnetic channel) are three-leg vertices. They can be obtained from the full, four-leg vertex function F through a sum over the left fermionic frequency v' . A diagrammatic representation of these three-leg vertices is shown in Fig. 3. With increasing order of non-locality the three-leg vertices read

$$\gamma_{r,lm m'l'}^{\omega v} = \sum_{n'h'v'} \chi_{0,lm n'h'}^{\omega v' v'} F_{r,h'n'm'l'}^{\omega v' v}, \quad (7)$$

$$\gamma_{r,lm m'l'}^{qv} = \sum_{n'h'v'} \chi_{0,lm n'h'}^{nl, qv' v'} F_{r,h'n'm'l'}^{\omega v' v}, \quad (8)$$

$$\eta_{r,lm m'l'}^{qv} = \sum_{n'h'v'} \chi_{0,lm n'h'}^{qv' v'} F_{r,h'n'm'l'}^{qv' v} - \gamma_{r,lm m'l'}^{\omega v}. \quad (9)$$

Thus, $\gamma^{\omega v}$ is a completely local three-leg vertex which can, in principle, be extracted directly from the impurity solver [36, 37]. If the DMFT impurity solver does not explicitly provide $\gamma^{\omega v}$, the latter is computed within the AbinitioDGA program according to Eq. (7).

The most complex ingredient of Eqs. (7)-(9) is the full four-leg vertex function $F_r^{\omega v' v}$ of the DMFT impurity model and its non-local counterpart $F_r^{qv' v}$. The former can be obtained from the connected part of the DMFT two-particle

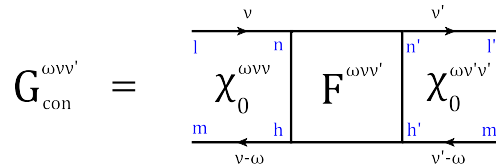


Figure 4: The local, full vertex function $F^{\omega v' v}$ can be obtained from the connected part of the two-particle impurity Green's function $G_{\text{con}}^{\omega v v'}$ through an 'amputation' of the left and the right legs [see Eq. (10)].

Green's function G^{con} , which is usually computed by the impurity solver [38, 39], through an 'amputation' of the left and the right legs (see Fig. 4), i.e. by multiplying with χ_0^{-1} from both sides. Explicitly, this yields

$$F_{r,lm m'l'}^{\omega \nu \nu'} = \sum_{nh n'h'} [(\chi_0^\omega)^{-1}]^{\nu \nu'}_{lm n'h'} G_{r,h'n'nh}^{\text{con } \omega \nu \nu'} [(\chi_0^\omega)^{-1}]^{\nu' \nu'}_{nh m'l'}. \quad (10)$$

The non-local, full vertex function $F_r^{\text{q}\nu \nu'}$ in Eq. (9) instead is obtained through the non-local version of the Bethe-Salpeter equation. However, as shown in Ref. [30], one can rewrite Eq. (9) in the compact form

$$\eta_{r,lm m'l'}^{\text{q}\nu} = \sum_{nh \nu'} (\vec{\mathbf{1}}_{lm hn} + \gamma_{r,lm hn}^{\omega \nu'}) \left\{ \left[\left(\mathbf{1} - \chi_0^{nl,q} F_r^\omega - 2\beta^{-2} \chi_0^q V^q (\mathbf{1} + \gamma_r^\omega) \delta_{rd} \right)^{-1} \right]^{\nu' \nu} - \mathbf{1}_{nh m'l'} \right\}, \quad (11)$$

where $\vec{\mathbf{1}}_{lm hn} = \delta_{ln} \delta_{mh}$. Thus, $\eta_r^{\text{q}\nu}$ can be computed efficiently through a single matrix inversion and a consecutive multiplication with the three-leg quantity $(\vec{\mathbf{1}} + \gamma_r^{\omega \nu'})$ from the left. Note that the matrix that is inverted has a compound index consisting of one fermionic frequency and two orbitals for both, row and column [cf. the indices $\{hn, \nu'\}$ and $\{m'l', \nu\}$ after the inversion in Eq. (11)]. In the expression that is inverted instead, orbital and fermionic frequency indices have been omitted for clarity. For more details we refer the reader to Section 4.2 and Fig. 9 (F^ω), Fig. 10 ($\chi_0^{nl,q}, \chi_0^q$), and Figs. 12, 13 (γ^ω, V^q). Please also note that, by neglecting $\hat{V}^{\mathbf{k}'-\mathbf{k}}$, the non-local Coulomb interaction V^q needs to be added only in the density channel.

2.2. Momentum-dependent susceptibilities

With the AbinitioDFA program one can also compute momentum-dependent, physical DMFT susceptibilities. In fact, the susceptibilities in the density and magnetic channel $r \in \{d, m\}$ can be obtained from the three-leg vertices in Eqs. (7) and (9) according to

$$\chi_{r,lm m'l'}^q = \chi_{r,lm m'l'}^\omega + \beta^{-2} \sum_\nu \chi_{0,lm m'l'}^{nl,q\nu \nu'} + \beta^{-2} \sum_\nu \eta_{r,lm m'l'}^{\text{q}\nu} \chi_{0,h'n'm'l'}^{q\nu \nu'} + \beta^{-2} \sum_\nu \gamma_{r,lm m'l'}^{\omega \nu} \chi_{0,h'n'm'l'}^{nl,q\nu \nu'}, \quad (12)$$

where $\chi_{r,lm m'l'}^\omega$ is the purely local DMFT susceptibility defined as the sum of the unconnected and the connected contributions

$$\chi_{r,lm m'l'}^\omega = \beta^{-2} \sum_\nu \chi_{0,lm m'l'}^{\omega \nu \nu'} + \beta^{-2} \sum_{\nu \nu'} G_{r,lm m'l'}^{\text{con } \omega \nu \nu'}. \quad (13)$$

The χ_0 bubble terms in Eqs. (12) and (13) are the ones defined in Eqs. (3)-(5). Please also note that the combined index q in Eq. (12) contains the momentum \mathbf{q} and the bosonic frequency ω . The magnetic susceptibility, e.g., in form of a spin-spin correlation function can then be obtained from Eq. (12) by summing over the corresponding orbital combinations $\chi_m^q = \sum_{ll'} \chi_{m,ll'l'}^q$. The thus calculated susceptibility is the q -dependent DMFT susceptibility. For calculating distinct DFA susceptibilities a self-consistency or λ -correction [32] is needed.

3. Program structure

In the previous Section, we have introduced the main equations implemented in the AbinitioDFA program. In this Section, we will focus on the structure and the usage of the program, before discussing some algorithmic details in Section 4. The AbinitioDFA work-flow is depicted in Fig. 5. There, all important program and file names are given. In the following, we will discuss all necessary steps, which can be grouped into the initial DFT+DMFT computation (Section 3.1), the preprocessing of the DMFT two-particle Green's function (Section 3.2) and the execution of the main AbinitioDFA program (Section 3.3).

3.1. DFT+DMFT computation

As Fig. 5 shows, the starting point of AbinitioDFA is a converged DFT+DMFT calculation for the material under investigation. Here, we use the Wien2k program package [40, 41] to perform the DFT computation, the wien2wannier interface [42] and wannier90 [43] to construct the Wannier Hamiltonian $H_W^{\mathbf{k}}$, and the w2dynamics program [44, 45] which solves the DMFT impurity model by continuous-time quantum Monte Carlo simulations in the hybridization

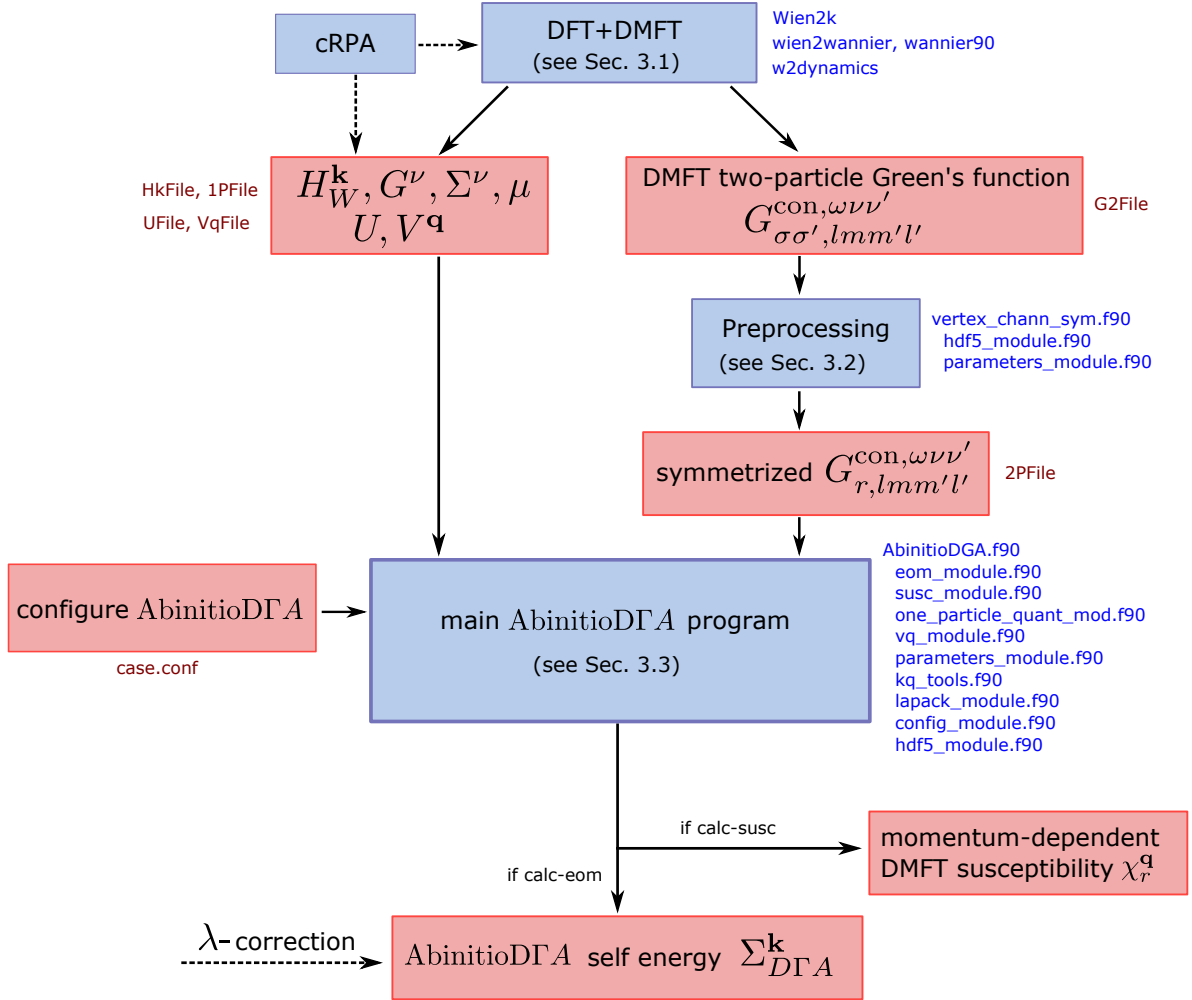


Figure 5: Flow diagram of the AbinitioDGA algorithm. Programs are indicated as blue boxes with the main program and module names listed on the right. The input/output data files instead are indicated in red.

expansion (CT-HYB) [46, 47, 48]. However, with the AbinitioDFA distribution, a python tool `dmft2adga-input.py` is provided that allows to swiftly interface the present code to other DMFT packages.

The initial DFT+DMFT computation provides all one-particle quantities used in AbinitioDFA: the Wannier Hamiltonian H_W^k , the local DMFT one-particle Green's function G^v and self-energy Σ^v , as well as the chemical potential μ . H_W^k , Σ^v and μ are needed to compute the non-local DMFT Green's function in Eq. (2) and the corresponding bubble-term in Eq. (4), while the local DMFT Green's function G^v is used to construct the local bubble-term in Eq. (3). The Wannier Hamiltonian H_W^k is stored in the file `HkFile`, while all the other DMFT single-particle quantities can be found in the hierarchical data format (hdf5) file `1PFile`.

The local and non-local Coulomb interaction U and V^q can also be obtained *ab initio* by using the constrained random phase approximation (cRPA) [49, 50]. The four-index U and V^q are stored in the files `UFile` and `VqFile` respectively.

After convergence of the DFT+DMFT cycle, the connected part of the DMFT two-particle Green's function G^{con} is computed, which is a numerically very demanding task. In practice, G^{con} is computed within the `w2dynamics` program package by extending the continuous time CT-HYB with a worm algorithm and improved estimators [38, 39]. Recently, vertex asymptotics have been implemented within `w2dynamics` [37]. Thus, the high-frequency asymptotics of the local, full vertex function $F^{\omega\nu\nu'}$ are directly computed within CT-HYB by considering all asymptotically contributing diagrams. This reduces statistical uncertainties of the local vertex and allows us to extend the fermionic and bosonic frequency boxes. The multi-orbital G^{con} requires a lot of storage capacity: $2^4 \#o^4 \# \omega^3$ double complex numbers, where $\#o$ is the number of orbitals and $\#\omega$ the number of Matsubara frequencies. In order to minimize the amount of storage, we store only its non-zero spin-orbital components in the hdf5 file `G2File` in the form of a lookup-table (for details please refer to Section 4.1).

3.2. Preprocessing of the DMFT two-particle Green's function

Before starting the main AbinitioDFA program, the file `G2File` containing the connected part of the two-particle impurity Green's function G^{con} is pre-processed by the program `vertex_chann_sym.f90`. This serves three purposes:

1. Symmetry-equivalent elements are averaged to improve on the statistics of G^{con} . Currently implemented are SU(2) symmetry (which in the present version is always assumed) and (full) orbital symmetries which are enforced if the corresponding flag is on.
2. G^{con} is transformed into the density and magnetic channel. In the paramagnetic and SU(2)-symmetric case, this can simply be achieved by computing

$$G_d^{\text{con}} = \frac{1}{2} (G_{\uparrow\uparrow\uparrow\uparrow}^{\text{con}} + G_{\downarrow\downarrow\downarrow\downarrow}^{\text{con}} + G_{\uparrow\uparrow\downarrow\downarrow}^{\text{con}} + G_{\downarrow\downarrow\uparrow\uparrow}^{\text{con}}), \quad (14)$$

$$G_m^{\text{con}} = \frac{1}{2} (G_{\uparrow\downarrow\downarrow\uparrow}^{\text{con}} + G_{\downarrow\uparrow\uparrow\downarrow}^{\text{con}}). \quad (15)$$

3. The symmetrized G_r^{con} in the density and magnetic channel is written into `2PFile` whose data structure is optimized for parallel access of the main program.

3.3. The main AbinitioDFA program

Configuration. The AbinitioDFA program uses a free-format configuration file. Here, we briefly describe the major options and keywords; for a full documentation, see the code repository.

The input of the AbinitioDFA program consists of four major parts, see Fig. 5:

1. The Wannier Hamiltonian (in the format of `wien2wannier`) is specified in `HkFile`. The latter contains the full H_W^k in the reducible Brillouin zone. The number of impurities as well as the number of k-points in each direction is required as additional input, since this information is not provided in the current `wien2wannier` file format. The orbital structure (correlated and ligand orbitals) is specified in the `w2dynamics` input format.
2. The local Coulomb interaction (computed, e.g., within cRPA) is either provided as a four-index object $U_{lm'm'l'}$ in a text file `UFile`, or is given as parameters `Udd`, `Jdd`, etc. and used in a Kanamori or density-density parametrization set in `Interaction`. Besides the local interaction used in the DMFT, a completely non-local interaction (V^q , with $\sum_q V^q = 0$) can be specified in the `VqFile`. The latter is a hdf5-file which contains only the non-zero spin-orbital components of V^q in the form of a lookup table.

3. The converged DMFT run in w2dynamics-style hdf5-format is specified as `1PFile`. The latter supplies all additional information that is required to build the one-particle Greens function of Eq.(2), i.e. the (inverse) temperature β , the chemical potential μ , the double-counting correction Σ_{DC} , and the DMFT self-energy Σ^v .
4. Finally, as the centerpiece of AbinitioDGA the two-particle Green's function calculated on top of the DMFT solution is specified in `2PFile`. This hdf5-file provides the symmetrized form of the two-particle Greens function in the density and magnetic channel, and is generated by the preprocessing program `vertex_chann_sym.f90`, as described in Section 3.2.

With this input one can then choose to compute the AbinitioDGA self-energy via the equation of motion `calc-eom` and/or momentum-dependent susceptibilities by setting `calc-susc` to true.

Execution. After the installation and configuration (for details see the code repository), the AbinitioDGA program can be executed by

```
mpirun -np N ./AbinitioDGA case.conf
```

where N is the total number of processor cores. Each core processes a different range of q -indices and reads in only the data slices of `2PFile` that it actually needs. Indeed, the three-leg vertices $\gamma^{\omega\nu}$, γ^{qv} and η^{qv} in Eqs. (7)-(9) can be computed independently for each q . Finally, in the equation of motion Eq. (1) all q -contributions are summed over. Also the q -dependent susceptibilities of Eq. (12) can be computed separately for each q . Hence, the main AbinitioDGA program `AbinitioDGA.f90` is MPI-parallelized over the combined bosonic index $q = (\mathbf{q}, \omega)$ and does not require any heavy inter-process communication.

The main AbinitioDGA program `AbinitioDGA.f90` is split into several modules. These are listed on the right hand side of Fig. 5. There exists a module for the computation of the equation of motion `eom_module.f90`, and one for computing the momentum-dependent susceptibilities `susc_module.f90`. All subroutines involving one-particle Green's functions and non-interacting susceptibilities χ_0 are gathered in the module `one_particle_quant_mod.f90`. The module `vq_module.f90` contains routines related to the local and non-local Coulomb interaction. Furthermore, the module `parameters_module.f90` specifies global parameters and quantities. Several routines regarding k -point operations, e.g the efficient search for the index of $\mathbf{k} - \mathbf{q}$, are gathered in `kq_tools.f90`. Finally, the module `lapack_module.f90` contains a wrapper for LAPACK-based matrix inversions, `config_module.f90` manages the input, and `hdf5_module.f90` provides routines dealing with the reading from or writing to hdf5-files (the same hdf5-module is also used by the preprocessing script).

Output. As well as for the input, the AbinitioDGA program utilizes the hdf5 file format also for its main output. Besides reducing hard-disk memory requirements with respect to text files, the hdf5 format also facilitates slicing and plotting of multi-dimensional arrays. The name of the output file contains the time stamp of the start of the computation in order to make its name unique and identifiable. At top-level, the file contains three groups (see Fig. 6):

1. `input` consists of several datasets, in which the DFT+DMFT input data (but not the two-particle Green's function) are stored. This is done merely for convenience, so as to simplify, e.g., comparisons of the DMFT self-energy (stored in `input/siw`) versus the AbinitioDGA self-energy.
2. `susceptibility` contains groups for both the local (`loc`) and non-local (`nonloc`) DMFT-susceptibility of Eqs. (12) and (13). Each of these subgroups contains three datasets: `bubble` for the susceptibility without vertex corrections, `dens` for the charge susceptibility (i. e. density channel), and `magn` for the spin susceptibility (i.e. magnetic channel). Local susceptibilities are stored as five-dimensional arrays, where the bosonic Matsubara frequency is the first index, followed by four orbital indices, in the usual order that is used also in the formulas throughout this paper. The non-local susceptibilities are stored in eight-dimensional arrays, consisting of frequency index, momentum vector $\mathbf{q} = (q_x, q_y, q_z)$ and four orbital indices.
3. `selfenergy` contains the AbinitioDGA self-energy Σ_{DGA}^k of Eq. (1) in the subgroup `nonloc/dga`. Here Σ_{DGA}^k is stored as a five-dimensional array with a fermionic frequency, three momenta, and two band indices. Please note, however, that the Σ_{DGA}^k stored in `nonloc/dga` does not contain the non-local part of the Hartree-Fock term Σ_{HF}^k of Eq. (6), which is stored separately in `nonloc/hartree_fock`. The subgroup `loc/dga_ksum` contains the local (\mathbf{k} -summed) AbinitioDGA self-energy $\Sigma_{DGA}^v = \sum_{\mathbf{k}} \Sigma_{DGA}^k$. Furthermore, `loc/dmft` contains the DMFT self-energy obtained through the local version of the equation of

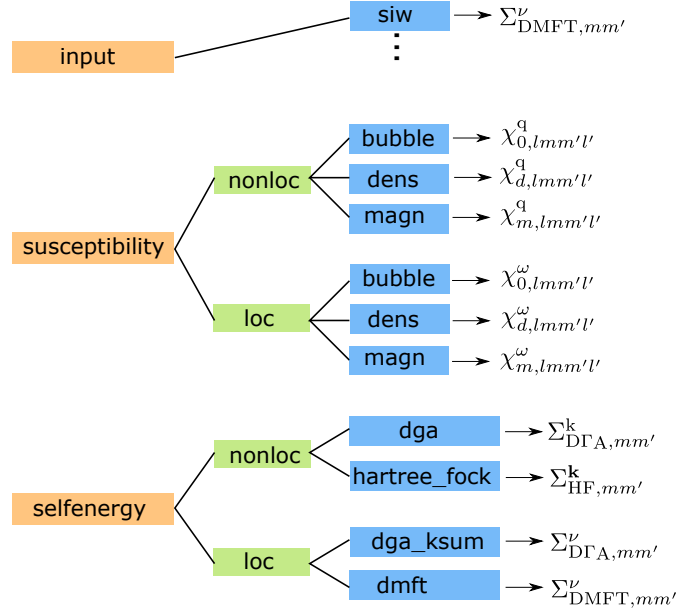


Figure 6: Group structure of the AbinitioDFA output.

motion, i.e. $\Sigma_{\text{DMFT}}^\nu = -\beta^{-1} \sum_\omega U \gamma_d^{\omega\nu} G^{\nu-\omega}$. Up to statistical fluctuations, the latter coincides with the 'original' DMFT self-energy stored in input/siw. A cross-check of input/siw with selfenergy/loc/dmft is always recommended.

4. Algorithmic details

4.1. Storage of the DMFT two-particle Green's function

The connected part of the DMFT two-particle Green's function G^{con} , which can be measured e.g., in CT-HYB, is a very large quantity and needs a lot of storage capacity. In its most general form G^{con} has four orbital indices $lmm'l'$ and four spin indices $\sigma_1\sigma_2\sigma_3\sigma_4$, and it depends on three Matsubara frequencies $\omega\nu\nu'$: $G_{\sigma_1\sigma_2\sigma_3\sigma_4,lmm'l'}^{\text{con } \omega\nu\nu'}$. However, the orbital and spin degrees of freedom are restricted by the symmetries of the local DMFT impurity problem. The Kanamori parameterization of interactions allows only for orbital combinations with pairwise identical orbitals: (ijj, ijj, ijj) . Furthermore, in the SU(2)-symmetric and paramagnetic case, also the spin degrees of freedom are reduced. Hence, many spin-orbital components of $G_{\sigma_1\sigma_2\sigma_3\sigma_4,lmm'l'}^{\text{con } \omega\nu\nu'}$ are actually zero. Thus, the amount of storage for G^{con} can be massively reduced by storing only its non-zero spin-orbital components in the file G2File. This reduces the required storage space by a factor of $\frac{[2(\#o)]^4}{6[3(\#o)^2 - 2(\#o)]} \approx 10$ for the example calculation in Section 5.

Group structure of the G2File. The non-zero spin-orbital components of G^{con} are stored in the hdf5 file G2File in the form of a "lookup-table". This means that the band and spin indices of $G_{\sigma_1\sigma_2\sigma_3\sigma_4,lmm'l'}^{\text{con } \omega\nu\nu'}$ are translated into a single index Ω through a unique transformation (subroutines component2index and index2component, respectively):

$$\sigma_1\sigma_2\sigma_3\sigma_4, lmm'l' \leftrightarrow \Omega. \quad (16)$$

The index Ω is then used to store the non-zero spin-orbital components of G^{con} in G2file. That is, the index Ω is the name of the groups in G2File containing the corresponding non-zero spin-orbital component of G^{con} . Thus, G2File contains as many groups as there are non-zero spin-orbital components in G^{con} . For example, for SrVO₃ in a paramagnetic t_{2g} setup the structure of the G2File is shown in Fig. 7. The number of non-zero elements in G^{con} depends, in particular, on the type of interactions used. There is an increasing number of elements from density-density to Kanamori to full Coulomb interaction.

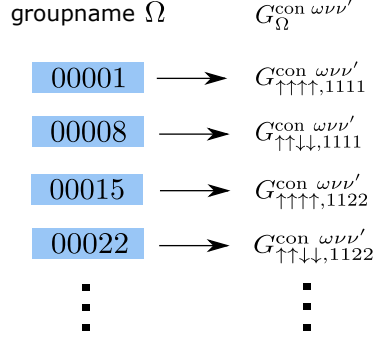


Figure 7: Structure of the G2File, which contains the two-particle (connected) impurity Green's function G^{con} . Each group—named by the combined index Ω —contains the corresponding non-zero spin-orbital component of G^{con} . Shown are the first four groups in the SrVO₃ example file. Note that many spin-orbital combinations do not exist and are hence not stored, e.g., $\Omega = 2$ which corresponds to $G_{\uparrow\uparrow\downarrow\downarrow,1111}^{\text{con } \omega\nu\nu'}$.

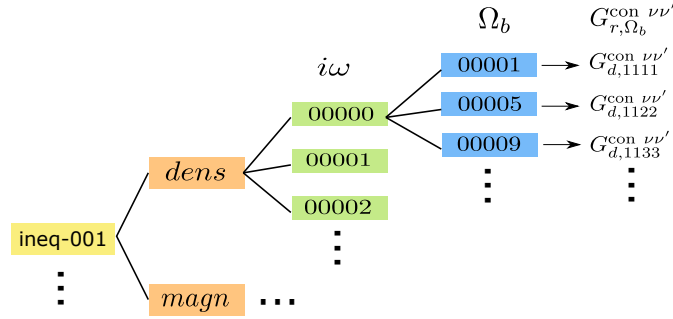


Figure 8: Group structure of the 2PFile, which contains the SU(2)- and orbital-symmetrized G^{con} in the density and magnetic channel. $i\omega$ refers to the bosonic frequency index, while Ω_b is a combined index of the four orbital indices $lmm'l'$. Shown are the first few entries in the SrVO₃ file (three orbitals, Kanamori interaction).

Group structure of the 2PFile. The preprocessing program `vertex_chann_sym.f90` symmetrizes the two-particle Green's function stored in G2File and transforms it into the density and magnetic channel $r \in \{d, m\}$. The symmetrized G_r^{con} is then written into the file 2PFile. The group structure of the latter is shown in Fig. 8. The file contains groups for inequivalent atoms, and subsequent groups for the density and the magnetic channel. As the AbinitioDΓA algorithm is parallelized over the bosonic Matsubara frequency, the data is further split in subgroups for each ω , allowing for an improved read-in of a given bosonic frequency slice of G_r^{con} . Each bosonic frequency group finally contains subgroups with the non-zero orbital components of $G_{r,lmm'l'}^{\text{con } \nu\nu'}$. These orbital subgroups are labeled by the combined orbital index Ω_b . The latter is defined through a similar index transformation as in Eq. (16), but involving only the four orbital indices, i.e.,

$$lmm'l' \leftrightarrow \Omega_b. \quad (17)$$

Due to the mapping of six spin components into the two channels [see Eqs.(14)-(15)], the size of the 2PFile is only about one third of the initial G2File.

4.2. Compound indices and matrix operations

In order to efficiently perform the orbital and frequency summations, we introduce compound indices so as to write the equations presented in Section 2 as matrix operations. The compound indices are obtained by transforming the four orbital and two fermionic frequency indices, e.g., of $F_{lmm'l'}^{\omega\nu\nu'}$, into two compound indices: the two left orbital indices lm and the left fermionic frequency index ν are combined into one compound index $\{ml, \nu\}$, while the two

$$F_{ml'l'm'}^{\nu\nu'} = \begin{matrix} & \{m'l', \nu'\} \\ & 11, \nu'_1 & 12, \nu'_1 & 21, \nu'_1 & 22, \nu'_1 & 11, \nu'_2 & 12, \nu'_2 & 21, \nu'_2 & 22, \nu'_2 & \dots \\ \{ml, \nu\} & 11, \nu_1 & F_{1111}^{\nu_1\nu'_1} & F_{1112}^{\nu_1\nu'_1} & F_{1121}^{\nu_1\nu'_1} & F_{1122}^{\nu_1\nu'_1} & & & & \\ & 12, \nu_1 & F_{2111}^{\nu_1\nu'_1} & F_{2112}^{\nu_1\nu'_1} & F_{2121}^{\nu_1\nu'_1} & F_{2122}^{\nu_1\nu'_1} & & & & \\ & 21, \nu_1 & F_{1211}^{\nu_1\nu'_1} & F_{1212}^{\nu_1\nu'_1} & F_{1221}^{\nu_1\nu'_1} & F_{1222}^{\nu_1\nu'_1} & \blacksquare & \blacksquare & \blacksquare & \\ & 22, \nu_1 & F_{2211}^{\nu_1\nu'_1} & F_{2212}^{\nu_1\nu'_1} & F_{2221}^{\nu_1\nu'_1} & F_{2222}^{\nu_1\nu'_1} & & & & \\ & 11, \nu_2 & & & & & F_{1111}^{\nu_2\nu'_2} & & & \\ & 12, \nu_2 & & & & & \blacksquare & \blacksquare & & \\ & 21, \nu_2 & & \blacksquare & & & \blacksquare & \blacksquare & & \\ & 22, \nu_2 & & \blacksquare & & & & & & \\ & \vdots & & & & & & & & \end{matrix}$$

Figure 9: By using compound indices $\{ml, \nu\}$ and $\{m'l', \nu'\}$, $F_{lmm'l'}^{\omega\nu\nu'}$ can be written in matrix form (in the graphics, the "external" bosonic frequency ω has been omitted for simplicity). Explicitly shown is the first orbital block ($\nu = \nu_1, \nu' = \nu'_1$) for the case of two orbitals. Please note that many entries are zero if density-density or Kanamori interactions are employed, e.g., $F_{1112}^{\nu_1\nu'_1} = 0$ and $F_{1121}^{\nu_1\nu'_1} = 0$.

$$\chi_{0,lmm'l'}^{\nu\nu'} = \begin{matrix} & \{m'l', \nu'\} \\ & 11, \nu'_1 & 12, \nu'_1 & 21, \nu'_1 & 22, \nu'_1 & 11, \nu'_2 & 12, \nu'_2 & 21, \nu'_2 & 22, \nu'_2 & \dots \\ \{ml, \nu\} & 11, \nu_1 & \chi_{0,1111}^{\nu_1\nu'_1} & \chi_{0,1112}^{\nu_1\nu'_1} & \chi_{0,1121}^{\nu_1\nu'_1} & \chi_{0,1122}^{\nu_1\nu'_1} & & & & \\ & 12, \nu_1 & \chi_{0,2111}^{\nu_1\nu'_1} & \chi_{0,2112}^{\nu_1\nu'_1} & \chi_{0,2121}^{\nu_1\nu'_1} & \chi_{0,2122}^{\nu_1\nu'_1} & & & & \\ & 21, \nu_1 & \chi_{0,1211}^{\nu_1\nu'_1} & \chi_{0,1212}^{\nu_1\nu'_1} & \chi_{0,1221}^{\nu_1\nu'_1} & \chi_{0,1222}^{\nu_1\nu'_1} & & & & \\ & 22, \nu_1 & \chi_{0,2211}^{\nu_1\nu'_1} & \chi_{0,2212}^{\nu_1\nu'_1} & \chi_{0,2221}^{\nu_1\nu'_1} & \chi_{0,2222}^{\nu_1\nu'_1} & & & & \\ & 11, \nu_2 & & & & & \chi_{0,1111}^{\nu_2\nu'_2} & \chi_{0,1112}^{\nu_2\nu'_2} & \chi_{0,1121}^{\nu_2\nu'_2} & \chi_{0,1122}^{\nu_2\nu'_2} \\ & 12, \nu_2 & & & & & \chi_{0,2111}^{\nu_2\nu'_2} & \chi_{0,2112}^{\nu_2\nu'_2} & \chi_{0,2121}^{\nu_2\nu'_2} & \chi_{0,2122}^{\nu_2\nu'_2} \\ & 21, \nu_2 & & & & & \chi_{0,1211}^{\nu_2\nu'_2} & \chi_{0,1212}^{\nu_2\nu'_2} & \chi_{0,1221}^{\nu_2\nu'_2} & \chi_{0,1222}^{\nu_2\nu'_2} \\ & 22, \nu_2 & & & & & \chi_{0,2211}^{\nu_2\nu'_2} & \chi_{0,2212}^{\nu_2\nu'_2} & \chi_{0,2221}^{\nu_2\nu'_2} & \chi_{0,2222}^{\nu_2\nu'_2} \\ & \vdots & & & & & & & & \end{matrix}$$

Figure 10: Matrix structure of the bubble terms $\chi_{0,lmm'l'}^{nl,q\nu\nu'}$, $\chi_{0,lmm'l'}^{q\nu\nu'}$ and $\chi_{0,lmm'l'}^{\omega\nu\nu'}$ (in the graphics, the "external" bosonic index $q = (\mathbf{q}, \omega)$ has been omitted). Shown are the first two "orbital blocks" (in orange). The block-diagonal structure arises from the fact that the bubble terms are diagonal with respect to the fermionic frequency $\delta_{\nu\nu'}$. Here, the full structure is only shown for clarity, the main AbinitioDFA program stores and works only with the non-zero orbital blocks.

Figure 11: The matrix multiplication of the block-diagonal $\chi_0^{nl,q\nu\nu'}$ with the full $F_{r,lm\nu'l'}^{\omega\nu\nu'}$ in Eqs. (8) and (11) can be split into several smaller operations. By multiplying each orbital block of $\chi_0^{nl,q\nu\nu'}$ with the corresponding slice of $F_{r,lm\nu'l'}^{\omega\nu\nu'}$ (marked with the same color), multiplications with entries that are zero by construction can be avoided.

right orbital indices $m'l'$ and the right fermionic frequency index ν' form the second compound index $\{m'l', \nu'\}$.¹ This way, $F_{lm\nu'l'}^{\omega\nu\nu'}$ can be written in matrix form, $F_{\{m'l', \nu'\}\{ml, \nu\}}^{\omega}$, as illustrated in Fig. 9. Please note that in the local $F_{lm\nu'l'}^{\omega\nu\nu'}$ many matrix elements are zero, since the Kanamori interaction allows only for entries with pairwise matching orbitals. These zero matrix elements are exactly the orbital components not present in 2PFIle. However, in order to perform straightforward matrix operations, one needs to work with the whole matrix including all zero elements. On the other hand, this has the advantage that the implementation of the main AbinitioDFA program is not restricted to density-density or Kanamori kind of interactions.

Similar to the local, full vertex function $F^{\omega\nu\nu'}$, also the bubble terms $\chi_0^{nl,q\nu\nu'}$, $\chi_0^{q\nu\nu'}$ and $\chi_0^{\omega\nu\nu'}$ can be written in matrix form with respect to the compound indices $\{ml, \nu\}$ and $\{m'l', \nu'\}$, as visualized in Fig. 10. Since the bubble terms are diagonal with respect to the fermionic frequency indices $\chi_0^{\nu\nu'} = \chi_0^{\nu\nu'} \delta_{\nu\nu'}$, they have a block-diagonal structure in the compound basis.

Simplified matrix operations. The computation of the three-leg vertices γ^q and η^q in Eqs. (8) and (11) involves a multiplication of $\chi_0^{nl,q}$ with F^ω . This matrix multiplication can be simplified by exploiting the block-diagonal structure of $\chi_0^{nl,q}$. In fact, by multiplying each orbital block of $\chi_0^{nl,q}$ with the corresponding horizontal slice of F^ω , as shown in Fig. 11, one can avoid multiplications involving entries that are zero by construction.

The matrix inversion in the equation for η^q , Eq. (11), instead cannot make use of a block-diagonal structure so that the inversion of the full matrix is needed. From a numerical point of view, this matrix inversion is one of the most demanding operations in the main AbinitioDFA program.

The calculation of the three-leg vertices in Eqs. (7)-(11) furthermore requires a sum over the left fermionic frequency. The summation over this left fermionic frequency makes them, diagrammatically, *three-leg* (electron-boson) vertices. In terms of compound matrices, this sum over the left fermionic frequency is visualized in Fig. 12. Through the sum, the left compound index is reduced to an orbital compound index $\{lm\}$ and the resulting matrix is not quadratic any more. Please note that this summation over the left fermionic frequency needs to be performed explicitly only in order to obtain γ^q and γ^ω .² The three-leg structure of η^q is actually obtained in a different way, namely by multiplying with $(\vec{1} + \gamma^\omega)$ from the left, as can be seen in Eq. (11).

In the equation of motion (1), the three-leg vertices γ_r^ω , γ_r^q and η_r^q are multiplied with the corresponding local and non-local Coulomb interaction terms (U , \tilde{U} and V^q). In order to perform this operation in the basis of compound indices, the four-index $U_{lm\nu'l'}$ and $V_{lm\nu'l'}^q$ are transformed to compound indices $\{ml\}$ and $\{m'l'\}$. Then, the multiplication of V^q and U times the three-leg γ 's and η can be performed easily, as schematically depicted in Fig. 13.

The final convolution with the non-local Green's function G^{k-q} in the equation of motion (1) instead is more straightforward to perform by breaking up the compound indices into single orbital and frequency indices.

¹Note that the bosonic frequency ω does not enter the compound index; in fact, the AbinitioDFA program is parallelized over the "external" index $q = (\mathbf{q}, \omega)$.

²If the purely local three-leg vertex γ^ω is directly computed in CT-HYB, the current sum over the left fermionic frequency to obtain γ^ω is redundant.

$$\gamma^\omega, \gamma^q, \eta^q = \left\{ \begin{matrix} m, l \end{matrix} \right\} \left(\begin{array}{c} \begin{matrix} \nu_1' & \nu_2' & \dots \\ \nu_1' & \nu_2' & \dots \\ \nu_1' & \nu_2' & \dots \\ \nu_2' & \nu_2' & \dots \\ \nu_3' & \nu_2' & \dots \\ \vdots & \vdots & \ddots \end{matrix} \end{array} \right)$$

Figure 12: Schematic representation of the sum over the left fermionic frequency needed to obtain the three-leg vertices γ^ω , γ^q and η^q in Eqs. (7)-(11). By summing over all stacked slices (different colors symbolize different left fermionic frequencies ν_i), the first dimension of the matrix is reduced to the orbital-only compound index $\{lm\}$.

$$\left\{ \begin{matrix} m, l \end{matrix} \right\} \left(\begin{array}{c} \begin{matrix} m'', l'' \end{matrix} \\ U, V^q \end{array} \right) \times \left\{ \begin{matrix} m'', l'' \end{matrix} \right\} \left(\begin{array}{c} \begin{matrix} m', l', \nu' \end{matrix} \\ \gamma^\omega, \gamma^q, \eta^q \end{array} \right)$$

Figure 13: Schematic representation of the matrix multiplication between the interaction matrices U and V^q and the three-leg vertices γ_r^ω , γ_r^q and η_r^q . This operation is part of the Schwinger-Dyson equation of motion (1).

4.3. Numerical effort

Often the numerical effort for calculating the local vertex in CT-HYB is the computationally most demanding task of an AbinitioDFA calculation. The calculation of the vertex scales as $\beta^5(\#o)^4$ with a large prefactor because of the Monte-Carlo sampling (let us remind the reader that $\#o$ is the number of orbitals and $\#\omega \sim \beta$ the number of Matsubara frequencies). This scaling can be understood from the fact that we need to calculate $(\#\omega)^3(\#o)^4$ different components of the local vertex, and the update of the CT-HYB hybridization matrix requires $\sim \beta^2$ operations because the mean expansion order and hybridization matrix dimension is $\sim \beta$. Since we eventually calculate the self-energy with only one frequency and two orbitals, a higher noise level can be tolerated if $\#\omega$ and $\#o$ are large. Hence, in practice a weaker dependence on $\#\omega$ and $\#o$ is possible. Calculating the vertex for SrVO₃ with $\#o = 3$, $\#\omega = 120$ and $\beta = 10 \text{ eV}^{-1}$ took 150000 core h on an Intel Xeon E5-2650v2 (2.6 GHz, 16 cores per node). One can also employ the asymptotic form [37, 51, 52] of the vertex for large frequencies. This asymptotic part depends on only two frequencies and thus scales as $\beta^4(\#o)^4$. This way the full CT-QMC calculation of the three-frequency vertex can be restricted to a small frequency box, and room temperature calculations should be feasible.

Let us now turn to the main AbinitioDFA program itself which is parallelized over the compound index $q = (\mathbf{q}, \omega)$. This parallelization gives us a factor $\#q \# \omega$ for the numerical effort ($\#q$: number of \mathbf{q} -points). For each q -point, the numerically most costly task is the matrix inversion in Eq. (11). The dimension N of the matrix that needs to be inverted is $N = \#\omega(\#o)^2$. While simple matrix inversions scale as N^3 more efficient ones scale roughly as $N^{2.5}$.³ Hence, the overall effort is $\sim \#q \# \omega^{3.5} \# o^5$. The numerical effort for calculating the self-energy via the equation of motion (1), on the other hand, is $\sim \#q^2 \# \omega^2 \# o^6$ and only becomes the leading contribution at high temperatures and for a large number of q -points.

For the AbinitioDFA computation of SrVO₃ with $\#o = 3$ and $\#q = 20^3$, the numerical effort with respect to the number of Matsubara frequencies $\#\omega$ has explicitly been tested by performing computations with three different frequency box sizes: $\#\omega = 120$, $\#\omega = 240$ and $\#\omega = 400$. Fig. 14 shows the respective numerical effort in core h. From Fig. 14 it can be seen that the main AbinitioDFA program indeed roughly scales with $(\#\omega)^{3.5}$.

³The matrix inversion in Eq. (11) is performed by using the lapack routines `zgetrf` and `zgetri`, which compute the inverse of a matrix by triangular decomposition.

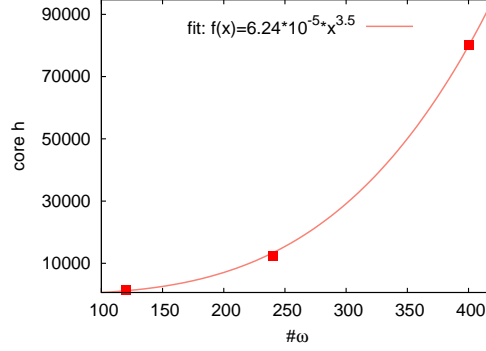


Figure 14: Computational effort of the AbinitioDFA program with respect to the number of involved Matsubara frequencies $\#\omega$.

5. Example case

As an example case we show momentum-dependent susceptibilities and AbinitioDFA self-energies for SrVO_3 . The latter is a strongly correlated transition metal oxide with a cubic perovskite crystal structure whose low-energy physics is dominated by its degenerate vanadium t_{2g} states. Experimentally, several manifestations of electronic correlations have been observed in SrVO_3 : photoemission spectroscopy [53] and specific heat measurements [54] find a mass enhancement of a factor of two compared to band-theory, the spectral function exhibits a satellite feature, i.e. a Hubbard band, below the quasiparticle peak [55, 53, 56], and at closer look a kink in the energy-momentum dispersion becomes visible [57, 58, 59]. Theoretically these phenomena have extensively been studied within various methods for strongly correlated electron systems. Indeed SrVO_3 has become a textbook example and testbed material in this field. Nonetheless, several physical aspects of this material are still under discussion and have recently been re-investigated with new, post-DMFT techniques. In fact, calculations that include the dynamical nature of the screened Coulomb interaction suggest that a sizable part of the mass enhancement in SrVO_3 originates from plasmon excitations [60, 61, 62, 63]. Furthermore, screened exchange contributions to the self-energy—that are caused by non-local interactions V^q —have been shown to compete with the mass enhancement from dynamical correlations [63, 64, 65]. Beside this academic interest, SrVO_3 has potential for technological applications, e.g., as an electrode material [66], Mott transistor [67] or transparent conductor [68]. Hence, SrVO_3 is a suitable target material for illustrating the capabilities and usage of our new AbinitioDFA algorithm.

5.1. AbinitioDFA self-energies for SrVO_3

In order to compute AbinitioDFA self-energies for SrVO_3 , the option `calc-eom` needs to be specified in the configuration file of the main AbinitioDFA program. Furthermore, the program must be provided with the Wannier Hamiltonian (stored in `HkFile`) and the one- and two-particle data (`1PFile` and `2PFile`) of a previous DFT+DMFT computation for SrVO_3 . The local and non-local Coulomb interaction instead are specified in the files `UFile` and `VqFile`. The results shown here, have been obtained [30] using only local Coulomb interactions in the Kanamori parametrization. Thus, it is sufficient to set the parameters `Udd = 5` and `Jdd = 0.75` in the `Interaction` part of the configuration file. This choice corresponds to an intra-orbital Coulomb interaction of $U = 5\text{eV}$ and an inter-orbital Hund's coupling of $J = 0.75\text{eV}$, as was used also in the required DFT+DMFT calculations. We further use an inverse temperature $\beta = 10\text{eV}^{-1}$.

With these input options, the k-dependent AbinitioDFA self-energies for SrVO_3 can be computed. Throughout the program, the default k-grid is the one of the wien2wannier Hamiltonian in `HkFile`, which is a regular k-grid in the reducible Brillouin zone of the material. Currently, AbinitioDFA self-energies can only be calculated for the k-points present in `HkFile`. For the SrVO_3 example case we chose a k-grid with $20 \times 20 \times 20$ k-points. The AbinitioDFA self-energies and corresponding spectral functions for four high-symmetry k-points are shown in Fig.15. In the two top panels, the real and imaginary part of the self-energy are displayed in color (red and blue) while the momentum-independent DMFT self-energy is shown in grey. Beside its k-dependence, the AbinitioDFA self-energy $\Sigma_{mm'}^k$ is also orbital-dependent: Different colors (red and blue) in Fig.15 refer to different orbitals $m = d_{xy}, d_{xz}, d_{yz}$. In general,

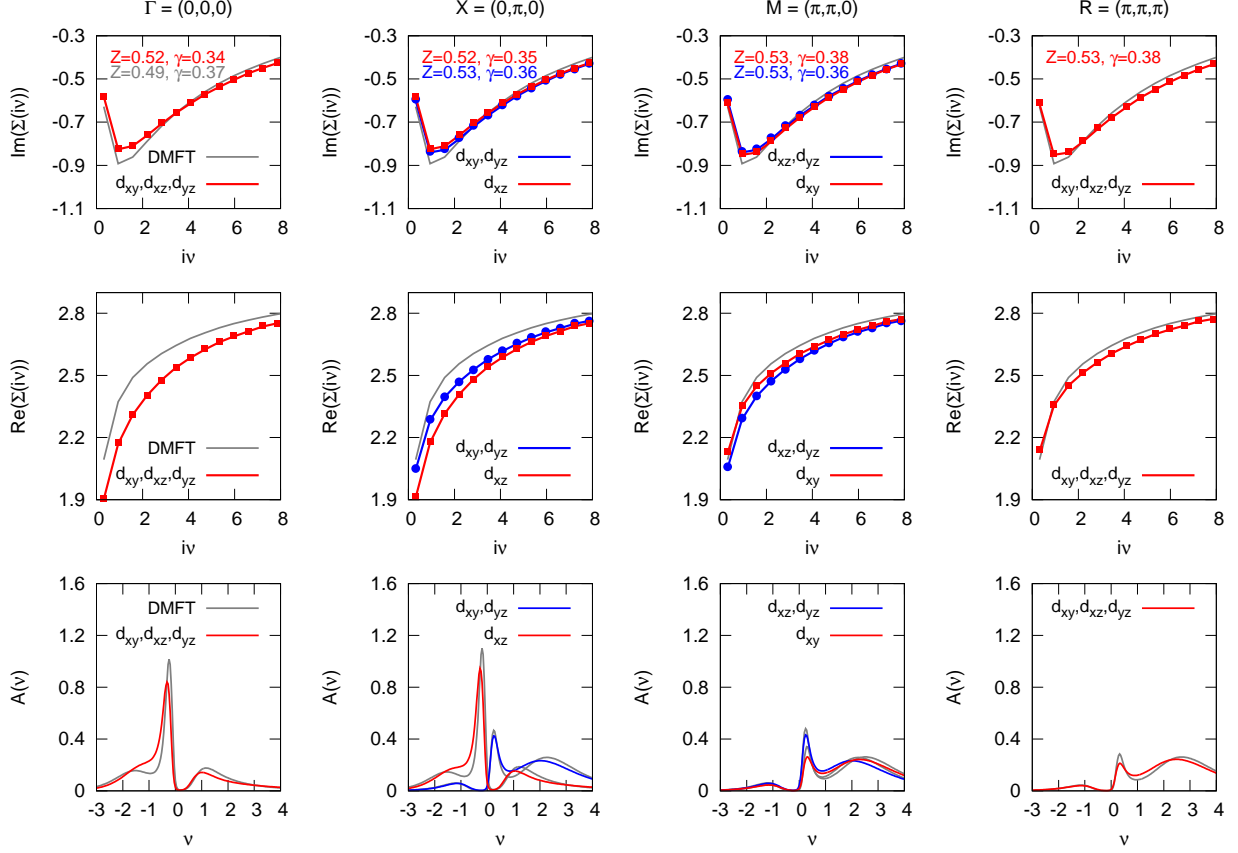


Figure 15: AbinitioDFA self-energies (top row: imaginary part, middle row: real part) and spectral functions (bottom row) for selected k-points in the Brillouin zone (Γ -point: first column, X -point: second column, M -point: third column, R -point: fourth column). In the two top panels, symbols indicate results for a small frequency box ($\#\omega/2 = 60$), while lines depict results for a large box ($\#\omega/2 = 200$): Congruence shows that the calculation is converged with respect to the number of frequencies.

also orbital-offdiagonal ($m \neq m'$) components of the self-energy can arise, except for high symmetry k-points. In this SrVO_3 example case however they are very small, so that we show only orbital-diagonal components.

Red (blue) *symbols* in the two top panels of Fig.15 refer to self-energies obtained with a frequency box of size $N = \#\omega/2 = 60$ corresponding to the range $[-i\nu_N : +i\nu_N]$ for fermionic and $[-i\omega_N : +i\omega_N]$ for bosonic frequencies. The results depicted by the red (blue) *lines* instead were obtained with a much larger box size of $\#\omega/2 = 200$. It can clearly be seen that both results lie on top of each other. However, it is always recommended to check the convergence of the AbinitioDFA results with respect to the employed frequency box sizes. For this purpose one can simply run a calculation with a smaller frequency box than the maximum default box which is the one of the local vertex function stored in 2PFile (here $\#\omega/2 = 200$). The smaller frequency box size of e.g., $\#\omega/2 = 60$ can simply be specified in the configuration file by setting $N4iwb = 60$ (bosonic frequency) and $N4iwf = 60$ (fermionic frequencies). The convergence of the AbinitioDFA self-energies with respect to the employed momentum-grid can instead be checked by reducing the number of q-points in the inner, parallel q-loop of the program (q_grid can be set to the desired number of q-points in the configuration file). In the present example case the results were checked to be perfectly converged for the employed grid.

From a physical point of view, the top panel of Fig.15 clearly shows that at low energies the imaginary part of the self-energy on the Matsubara axis is—for all orbitals and k-points—slightly smaller than in DMFT. As a result the scattering rate $\gamma = -\Im\Sigma(iv \rightarrow 0)$ very slightly decreases with respect to DMFT, while the quasi-particle weight Z_k increases. Besides this overall effect, the momentum dependence of $\Im\Sigma$ is small, which is a quite common finding

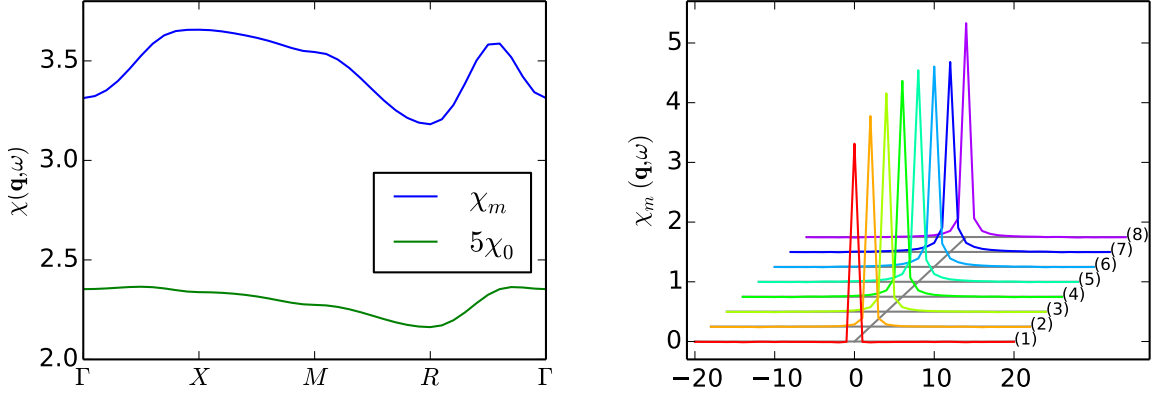


Figure 16: Magnetic susceptibilities of SrVO₃. Left: real part of the magnetic susceptibility χ_m at zero frequency, along a q-path connecting high-symmetry points in momentum space. For comparison, we also show the particle-hole bubble, χ_0 , scaled by a factor of 5. Right: real part of the dynamical magnetic susceptibility $\chi_m(i\omega_n)$ as a function of bosonic Matsubara frequencies $\omega_n = 2\pi n/\beta$ for 8 selected q-points: $\mathbf{q}_1 = (0,0,0)$, $\mathbf{q}_2 = (\pi/2,0,0)$, $\mathbf{q}_3 = (\pi,0,0)$, $\mathbf{q}_4 = (\pi,\pi/2,0)$, $\mathbf{q}_5 = (\pi,\pi,0)$, $\mathbf{q}_6 = (\pi,\pi,\pi/2)$, $\mathbf{q}_7 = (\pi,\pi,\pi)$, $\mathbf{q}_8 = (\pi/2,\pi/2,\pi/2)$. Please note that curves have been offset for better visibility.

within post-DMFT methods [69, 63, 70, 30]. The real-part of the self-energy instead shows larger deviations from the DMFT result. Indeed, at low energies the difference between AbinitioDΓA and DMFT reaches 200meV.

The bottom panels of Fig. 15 show the AbinitioDΓA spectral functions which were obtained by analytically continuing the Matsubara Green's function to the real-frequency axis through a maximum entropy algorithm. As expected from the analysis of the self-energies, also in the spectral functions we see signatures of reduced correlation effects compared to the DMFT results (in grey): Because of the larger Z-factor as well as $\Re\Sigma$ -induced shifts, the quasi-particle peaks move slightly away from the Fermi level while Hubbard bands are displaced towards it. For a more detailed discussion and physical interpretation of the results please refer to Ref. [30].

5.2. SrVO₃ susceptibilities

Since the calculation of DMFT susceptibilities employs the same Bethe-Salpeter ladder as in AbinitioDΓA, setting `calc-susc` to `true` only incurs little additional CPU costs. While it is recommended to use a large range of bosonic frequencies and a dense mesh of q-points for the computation of self-energies, there is more flexibility when calculating only susceptibilities. Namely, one can set `N4iwb` = 0 and `q_path_susc` = T to setup the computation of *static* susceptibilities along a q-path with potentially a large number of q-points. Results for the *static* DMFT susceptibility of SrVO₃ are shown in the left panel of Fig. 16, summed over all orbital contributions. There is only a weak momentum-dependence of the magnetic susceptibility in the high-temperature paramagnetic phase of SrVO₃, but vertex corrections strongly enhance the susceptibility by a factor of seven.

Indeed only if vertex corrections are taken into account the susceptibility agrees with the experimental value [71, 72]. For example, Ref. [71] reports $9.9\mu_B^2/\text{eV}^{-1}$ at 100K and $8.7\mu_B^2/\text{eV}^{-1}$ at 300K which, taken the temperature dependence into account, well agrees with our value of $6.7\mu_B^2/\text{eV}^{-1}$ at 1160K (for the conversion of units note that $1\mu_B^2/\text{eV} = 3.2327 \times 10^{-5}\text{emu/mol}$).

Alternatively, one can set `N4iwb` = 10 and reduce the number of q-points in order to produce the dynamical susceptibilities shown in the right panel of Fig. 16. These still need to be analytically continued to the physical (real frequency) dynamical susceptibilities. The susceptibilities on the Matsubara axis shown in Fig. 16 allow however for a better intercomparison and test case without the perils of analytical continuation, e. g. by the maximum entropy method.

6. Conclusion

In this paper we have outlined the structure of the AbinitioDFA program package and provided information on how to use it. While the numerical effort is considerably larger than for state-of-the-art DFT+DMFT calculations, our code makes realistic multi-orbital post-DMFT studies feasible. We expect AbinitioDFA calculations to provide valuable insight into the physics of non-local correlations in strongly correlated materials. Besides studying, e.g., the nature of non-local spin-fluctuations, our methodology also allows to systematically assess the error made in DFT+DMFT calculations.

Materials calculations with diagrammatic extensions of DMFT are just at the beginning. We believe that our code will contribute turning this route into a thriving research field, similar to what DFT+DMFT is today. We hope to foster this development by releasing the AbinitioDFA program package under the terms of the GNU General Public License version 3.

7. Acknowledgments

We would like to thank Patrik Gunacker for fruitful discussions and the cooperation on the SrVO₃ project. This work has been financially supported by the European Research Council under the European Union's Seventh Framework Program (FP/2007-2013) through ERC grant agreement n. 306447. Calculations have been done on the Vienna Scientific Cluster (VSC).

References

- [1] W. Metzner, D. Vollhardt, Correlated lattice fermions in $d = \infty$ dimensions, Phys. Rev. Lett. 62 (1989) 324–327. [doi:10.1103/PhysRevLett.62.324](#).
- [2] A. Georges, G. Kotliar, Hubbard model in infinite dimensions, Phys. Rev. B 45 (1992) 6479–6483. [doi:10.1103/PhysRevB.45.6479](#).
- [3] A. Georges, G. Kotliar, W. Krauth, M. J. Rozenberg, [Dynamical mean-field theory of strongly correlated fermion systems and the limit of infinite dimensions](#), Rev. Mod. Phys. 68 (1) (1996) 13. [doi:10.1103/RevModPhys.68.13](#).
URL <http://dx.doi.org/10.1103/RevModPhys.68.13>
- [4] E. Pavarini, E. Koch, D. Vollhardt, A. Lichtenstein, [DMFT at 25: Infinite Dimensions](#), Vol. 4 of Reihe Modeling and Simulation 4, Forschungszentrum Jülich Zentralbibliothek, Verlag (Jülich), Jülich, 2014.
URL <https://juser.fz-juelich.de/record/155829>
- [5] V. I. Anisimov, A. I. Poteryaev, M. A. Korotin, A. O. Anokhin, G. Kotliar, [First-principles calculations of the electronic structure and spectra of strongly correlated systems: dynamical mean-field theory](#), Journal of Physics: Condensed Matter 9 (1997) 7359–7367.
URL <http://stacks.iop.org/0953-8984/9/7359>
- [6] A. I. Lichtenstein, M. I. Katsnelson, Ab initio calculations of quasiparticle band structure in correlated systems: Lda++ approach, Phys. Rev. B 57 (1998) 6884–6895. [doi:10.1103/PhysRevB.57.6884](#).
- [7] P. Sun, G. Kotliar, [Extended dynamical mean-field theory and GW method](#), Phys. Rev. B 66 (2002) 085120. [doi:10.1103/PhysRevB.66.085120](#).
URL <http://link.aps.org/doi/10.1103/PhysRevB.66.085120>
- [8] S. Biermann, F. Aryasetiawan, A. Georges, [First-principles approach to the electronic structure of strongly correlated systems: Combining the gw approximation and dynamical mean-field theory](#), Phys. Rev. Lett. 90 (2003) 086402. [doi:10.1103/PhysRevLett.90.086402](#).
URL <http://link.aps.org/doi/10.1103/PhysRevLett.90.086402>
- [9] G. Kotliar, S. Y. Savrasov, K. Haule, V. S. Oudovenko, O. Parcollet, C. A. Marianetti, [Electronic structure calculations with dynamical mean-field theory](#), Rev. Mod. Phys. 78 (2006) 865. [doi:10.1103/RevModPhys.78.865](#).
URL <http://link.aps.org/doi/10.1103/RevModPhys.78.865>
- [10] K. Held, Electronic structure calculations using dynamical mean field theory, Advances in Physics 56 (2007) 829 – 926. [doi:10.1080/00018730701619647](#).
- [11] J. M. Tomczak, P. Liu, A. Toschi, G. Kresse, K. Held, [Merging gw with dmft and non-local correlations beyond](#), The European Physical Journal Special Topics 226 (11) (2017) 2565–2590. [doi:10.1140/epjst/e2017-70053-1](#).
URL <http://dx.doi.org/10.1140/epjst/e2017-70053-1>
- [12] M. H. Hettler, A. N. Tahvildar-Zadeh, M. Jarrell, T. Pruschke, H. R. Krishnamurthy, [Nonlocal dynamical correlations of strongly interacting electron systems](#), Phys. Rev. B 58 (1998) R7475–R7479. [doi:10.1103/PhysRevB.58.R7475](#).
URL <http://link.aps.org/doi/10.1103/PhysRevB.58.R7475>
- [13] A. I. Lichtenstein, M. I. Katsnelson, [Antiferromagnetism and \$d\$ -wave superconductivity in cuprates: A cluster dynamical mean-field theory](#), Phys. Rev. B 62 (2000) R9283–R9286. [doi:10.1103/PhysRevB.62.R9283](#).
URL <http://link.aps.org/doi/10.1103/PhysRevB.62.R9283>
- [14] G. Kotliar, S. Y. Savrasov, G. Pálsson, G. Biroli, [Cellular dynamical mean field approach to strongly correlated systems](#), Phys. Rev. Lett. 87 (2001) 186401. [doi:10.1103/PhysRevLett.87.186401](#).
URL <http://link.aps.org/doi/10.1103/PhysRevLett.87.186401>

- [15] T. Maier, M. Jarrell, T. Pruschke, M. H. Hettler, [Quantum cluster theories](#), Rev. Mod. Phys. 77 (2005) 1027. doi:10.1103/RevModPhys.77.1027.
URL <http://link.aps.org/doi/10.1103/RevModPhys.77.1027>
- [16] S. Biermann, A. Poteryaev, A. I. Lichtenstein, A. Georges, Dynamical singlets and correlation-assisted peierls transition in VO_2 , Phys. Rev. Lett. 94 (2005) 026404.
- [17] H. Lee, K. Foyevtsova, J. Ferber, M. Aichhorn, H. O. Jeschke, R. Valentí, [Dynamical cluster approximation within an augmented plane wave framework: Spectral properties of \$\text{SrVO}_3\$](#) , Phys. Rev. B 85 (2012) 165103. doi:10.1103/PhysRevB.85.165103.
URL <http://link.aps.org/doi/10.1103/PhysRevB.85.165103>
- [18] A. Toschi, A. A. Katanin, K. Held, Dynamical vertex approximation; a step beyond dynamical mean-field theory, Phys. Rev. B 75 (2007) 045118. doi:10.1103/PhysRevB.75.045118.
- [19] H. Kusunose, [Influence of spatial correlations in strongly correlated electron systems: Extension to dynamical mean field approximation](#), J. Phys. Soc. Jpn. 75 (5) (2006) 054713. doi:10.1143/JPSJ.75.054713.
URL <http://jpsj.ipap.jp/link?JPSJ/75/054713/>
- [20] A. N. Rubtsov, M. I. Katsnelson, A. I. Lichtenstein, Dual fermion approach to nonlocal correlations in the hubbard model, Phys. Rev. B 77 (2008) 033101. doi:10.1103/PhysRevB.77.033101.
- [21] G. Rohringer, A. Toschi, H. Hafermann, K. Held, V. I. Anisimov, A. A. Katanin, [One-particle irreducible functional approach: A route to diagrammatic extensions of the dynamical mean-field theory](#), Phys. Rev. B 88 (2013) 115112.
URL <http://link.aps.org/doi/10.1103/PhysRevB.88.115112>
- [22] C. Taranto, S. Andergassen, J. Bauer, K. Held, A. Katanin, W. Metzner, G. Rohringer, A. Toschi, [From infinite to two dimensions through the functional renormalization group](#), Phys. Rev. Lett. 112 (2014) 196402. doi:10.1103/PhysRevLett.112.196402.
URL <http://link.aps.org/doi/10.1103/PhysRevLett.112.196402>
- [23] T. Ayral, O. Parcollet, [Mott physics and spin fluctuations: a unified framework](#), Phys. Rev. B 92 (2015) 115109.
URL <http://link.aps.org/doi/10.1103/PhysRevB.92.115109>
- [24] G. Li, [Hidden physics in the dual-fermion approach: A special case of a nonlocal expansion scheme](#), Phys. Rev. B 91 (2015) 165134. doi:10.1103/PhysRevB.91.165134.
URL <http://link.aps.org/doi/10.1103/PhysRevB.91.165134>
- [25] G. Rohringer, A. Toschi, A. Katanin, K. Held, [Critical properties of the half-filled hubbard model in three dimensions](#), Phys. Rev. Lett. 107 (2011) 256402. doi:10.1103/PhysRevLett.107.256402.
URL <http://link.aps.org/doi/10.1103/PhysRevLett.107.256402>
- [26] D. Hirschmeier, H. Hafermann, E. Gull, A. I. Lichtenstein, A. E. Antipov, [Mechanisms of finite temperature magnetism in the three-dimensional hubbard model](#), Phys. Rev. B 92 (2015) 144409.
URL <http://dx.doi.org/10.1103/PhysRevB.92.144409>
- [27] A. E. Antipov, E. Gull, S. Kirchner, [Critical exponents of strongly correlated fermion systems from diagrammatic multiscale methods](#), Phys. Rev. Lett. 112 (2014) 226401. doi:10.1103/PhysRevLett.112.226401.
URL <http://link.aps.org/doi/10.1103/PhysRevLett.112.226401>
- [28] T. Schäfer, A. Katanin, K. Held, A. Toschi, [Quantum criticality with a twist - interplay of correlations and kohn anomalies in three dimensions](#), preprint [arXiv:1605.06355](https://arxiv.org/abs/1605.06355).
URL <http://arxiv.org/abs/1605.06355>
- [29] G. Rohringer, H. Hafermann, A. Toschi, A. A. Katanin, A. E. Antipov, M. I. Katsnelson, A. I. Lichtenstein, A. N. Rubtsov, K. Held, [Diagrammatic routes to non-local correlations beyond dynamical mean field theory](#), ArXiv e-prints [arXiv:arXiv:1705.00024](https://arxiv.org/abs/1705.00024).
- [30] A. Galler, P. Thunström, P. Gunacker, J. M. Tomczak, K. Held, [Ab initio](#), Phys. Rev. B 95 (2017) 115107. doi:10.1103/PhysRevB.95.115107.
URL <https://link.aps.org/doi/10.1103/PhysRevB.95.115107>
- [31] A. Galler, J. Kaufmann, P. Gunacker, P. Thunström, J. M. Tomczak, K. Held, [Towards ab initio calculations with the dynamical vertex approximation](#), ArXiv e-prints [arXiv:1709.02663](https://arxiv.org/abs/1709.02663).
- [32] A. A. Katanin, A. Toschi, K. Held, [Comparing pertinent effects of antiferromagnetic fluctuations in the two- and three-dimensional hubbard model](#), Phys. Rev. B 80 (2009) 075104. doi:10.1103/PhysRevB.80.075104.
URL <http://link.aps.org/doi/10.1103/PhysRevB.80.075104>
- [33] G. Rohringer, A. Toschi, [Impact of non-local correlations over different energy scales: A dynamical vertex approximation study](#), Phys. Rev. B 94 (2016) 125144. doi:10.1103/PhysRevB.94.125144.
URL <http://link.aps.org/doi/10.1103/PhysRevB.94.125144>
- [34] L. Hedin, [New method for calculating the one-particle green's function with application to the electron-gas problem](#), Phys. Rev. 139 (1965) A796–A823. doi:10.1103/PhysRev.139.A796.
URL <http://link.aps.org/doi/10.1103/PhysRev.139.A796>
- [35] J. Kuneš, R. Arita, P. Wissgott, A. Toschi, H. Ikeda, K. Held, [Wien2wannier: From linearized augmented plane waves to maximally localized wannier functions](#), Computer Physics Communications 181 (2010) 1888.
- [36] H. Hafermann, [Self-energy and vertex functions from hybridization-expansion continuous-time quantum monte carlo for impurity models with retarded interaction](#), Phys. Rev. B 89 (2014) 235128. doi:10.1103/PhysRevB.89.235128.
URL <https://link.aps.org/doi/10.1103/PhysRevB.89.235128>
- [37] J. Kaufmann, P. Gunacker, K. Held, [Continuous-time quantum monte carlo calculation of multiorbital vertex asymptotics](#), Phys. Rev. B 96 (2017) 035114. doi:10.1103/PhysRevB.96.035114.
URL <https://link.aps.org/doi/10.1103/PhysRevB.96.035114>
- [38] P. Gunacker, M. Wallerberger, E. Gull, A. Hausoel, G. Sangiovanni, K. Held, [Continuous-time quantum monte carlo using worm sampling](#), Phys. Rev. B 92 (2015) 155102. doi:10.1103/PhysRevB.92.155102.
URL <https://link.aps.org/doi/10.1103/PhysRevB.92.155102>

- [39] P. Gunacker, M. Wallerberger, T. Ribic, A. Hausoel, G. Sangiovanni, K. Held, *Worm-improved estimators in continuous-time quantum monte carlo*, Phys. Rev. B 94 (2016) 125153. doi:10.1103/PhysRevB.94.125153.
URL <https://link.aps.org/doi/10.1103/PhysRevB.94.125153>
- [40] P. Blaha, K. Schwarz, P. Sorantin, S. B. Trickey, *Full-potential, linearized augmented plane wave programs for crystalline systems*, Computer Physics Communications 59 (2) (1990) 399 – 415.
URL <http://www.sciencedirect.com/science/article/pii/0010465590901876>
- [41] K. Schwarz, P. Blaha, *Solid state calculations using wien2k*, Comp. Mater. Sci. 28 (2003) 259.
- [42] J. Kunes, R. Arita, P. Wissgott, A. Toschi, H. Ikeda, K. Held, *Wien2wannier: From linearized augmented plane waves to maximally localized Wannier functions*, Computer Physics Communications 181 (11) (2010) 1888–1895.
URL <http://www.sciencedirect.com/science/article/pii/S0010465510002948>
- [43] A. A. Mostofi, J. R. Yates, Y. S. Lee, I. Souza, D. Vanderbilt, N. Marzari, *wannier90: A tool for obtaining maximally-localised Wannier functions*, Computer Physics Communications 178 (9) (2008) 685–699.
URL <http://www.sciencedirect.com/science/article/pii/S0010465507004936>
- [44] N. Parragh, A. Toschi, K. Held, G. Sangiovanni, *Conserved quantities of $SU(2)$ -invariant interactions for correlated fermions and the advantages for quantum Monte Carlo simulations*, Phys. Rev. B 86 (2012) 155158.
URL <http://link.aps.org/doi/10.1103/PhysRevB.86.155158>
- [45] M. Wallerberger, PhD Thesis, TU Wien, 2016.
- [46] P. Werner, A. Comanac, L. de’ Medici, M. Troyer, A. J. Millis, *Continuous-time solver for quantum impurity models*, Phys. Rev. Lett. 97 (2006) 076405. doi:10.1103/PhysRevLett.97.076405.
URL <http://link.aps.org/doi/10.1103/PhysRevLett.97.076405>
- [47] P. Werner, A. J. Millis, *Hybridization expansion impurity solver: General formulation and application to kondo lattice and two-orbital models*, Phys. Rev. B 74 (2006) 155107. doi:10.1103/PhysRevB.74.155107.
URL <http://link.aps.org/doi/10.1103/PhysRevB.74.155107>
- [48] E. Gull, A. J. Millis, A. I. Lichtenstein, A. N. Rubtsov, M. Troyer, P. Werner, *Continuous-time monte carlo methods for quantum impurity models*, Rev. Mod. Phys. 83 (2) (2011) 349. doi:10.1103/RevModPhys.83.349.
URL <http://link.aps.org/doi/10.1103/RevModPhys.83.349>
- [49] F. Aryasetiawan, M. Imada, A. Georges, G. Kotliar, S. Biermann, A. I. Lichtenstein, *Frequency-dependent local interactions and low-energy effective models from electronic structure calculations*, Phys. Rev. B 70 (2004) 195104. doi:10.1103/PhysRevB.70.195104.
URL <https://link.aps.org/doi/10.1103/PhysRevB.70.195104>
- [50] T. Miyake, F. Aryasetiawan, *Screened coulomb interaction in the maximally localized wannier basis*, Phys. Rev. B 77 (2008) 085122. doi:10.1103/PhysRevB.77.085122.
URL <https://link.aps.org/doi/10.1103/PhysRevB.77.085122>
- [51] G. Li, N. Wentzell, P. Pudleiner, P. Thunström, K. Held, *Efficient implementation of the parquet equations: Role of the reducible vertex function and its kernel approximation*, Phys. Rev. B 93 (2016) 165103. doi:10.1103/PhysRevB.93.165103.
URL <https://link.aps.org/doi/10.1103/PhysRevB.93.165103>
- [52] N. Wentzell, G. Li, A. Tagliavini, C. Taranto, G. Rohringer, K. Held, A. Toschi, S. Andergassen, *High-frequency asymptotics of the vertex function: diagrammatic parametrization and algorithmic implementation*, arxiv:1610.06520.
URL <https://arxiv.org/abs/1610.06520>
- [53] A. Sekiyama, H. Fujiwara, S. Imada, S. Suga, H. Eisaki, S. I. Uchida, K. Takegahara, H. Harima, Y. Saitoh, I. A. Nekrasov, G. Keller, D. E. Kondakov, A. V. Kozhevnikov, T. Pruschke, K. Held, D. Vollhardt, V. I. Anisimov, *Mutual experimental and theoretical validation of bulk photoemission spectra of $\text{Sr}_{1-x}\text{Ca}_x\text{VO}_3$* , Phys. Rev. Lett. 93 (15) (2004) 156402. doi:10.1103/PhysRevLett.93.156402.
- [54] I. H. Inoue, O. Goto, H. Makino, N. E. Hussey, M. Ishikawa, *Bandwidth control in a perovskite-type $3d^1$ -correlated metal $\text{Ca}_{1-x}\text{Sr}_x\text{VO}_3$. i. evolution of the electronic properties and effective mass*, Phys. Rev. B 58 (1998) 4372–4383. doi:10.1103/PhysRevB.58.4372.
URL <http://link.aps.org/doi/10.1103/PhysRevB.58.4372>
- [55] K. Morikawa, T. Mizokawa, K. Kobayashi, A. Fujimori, H. Eisaki, S. Uchida, F. Iga, Y. Nishihara, *Spectral weight transfer and mass renormalization in mott-hubbard systems SrVO_3 and CaVO_3 : Influence of long-range coulomb interaction*, Phys. Rev. B 52 (1995) 13711–13714. doi:10.1103/PhysRevB.52.13711.
URL <https://link.aps.org/doi/10.1103/PhysRevB.52.13711>
- [56] M. Takizawa, M. Minohara, H. Kumigashira, D. Toyota, M. Oshima, H. Wadati, T. Yoshida, A. Fujimori, M. Lippmaa, M. Kawasaki, H. Koinuma, G. Sordi, M. Rozenberg, *Coherent and incoherent d band dispersions in SrVO_3* , Phys. Rev. B 80 (2009) 235104. doi:10.1103/PhysRevB.80.235104.
URL <http://link.aps.org/doi/10.1103/PhysRevB.80.235104>
- [57] I. A. Nekrasov, K. Held, G. Keller, D. E. Kondakov, T. Pruschke, M. Kollar, O. K. Andersen, V. I. Anisimov, D. Vollhardt, *Momentum-resolved spectral functions of SrVO_3 calculated by LDA + DMFT*, Phys. Rev. B 73 (2006) 155112. doi:10.1103/PhysRevB.73.155112.
URL <http://link.aps.org/doi/10.1103/PhysRevB.73.155112>
- [58] S. Aizaki, T. Yoshida, K. Yoshimatsu, M. Takizawa, M. Minohara, S. Ideta, A. Fujimori, K. Gupta, P. Mahadevan, K. Horiba, H. Kumigashira, M. Oshima, *Self-energy on the low- to high-energy electronic structure of correlated metal SrVO_3* , Phys. Rev. Lett. 109 (2012) 056401. doi:10.1103/PhysRevLett.109.056401.
URL <http://link.aps.org/doi/10.1103/PhysRevLett.109.056401>
- [59] K. Held, R. Peters, A. Toschi, *Poor man’s understanding of kinks originating from strong electronic correlations*, Phys. Rev. Lett. 110 (2013) 246402. doi:10.1103/PhysRevLett.110.246402.
URL <http://link.aps.org/doi/10.1103/PhysRevLett.110.246402>
- [60] M. Casula, A. Rubtsov, S. Biermann, *Dynamical screening effects in correlated materials: Plasmon satellites and spectral weight transfers from a green’s function ansatz to extended dynamical mean field theory*, Phys. Rev. B 85 (2012) 035115. doi:10.1103/PhysRevB.85.035115.

- URL <http://link.aps.org/doi/10.1103/PhysRevB.85.035115>
- [61] J. M. Tomczak, M. Casula, T. Miyake, F. Aryasetiawan, S. Biermann, **Combined gw and dynamical mean-field theory: Dynamical screening effects in transition metal oxides**, EPL (Europhysics Letters) 100 (6) (2012) 67001.
URL <http://stacks.iop.org/0295-5075/100/i=6/a=67001>
- [62] R. Sakuma, P. Werner, F. Aryasetiawan, **Electronic structure of srvo₃ within gw+dmft**, Phys. Rev. B 88 (2013) 235110. doi:10.1103/PhysRevB.88.235110.
URL <http://link.aps.org/doi/10.1103/PhysRevB.88.235110>
- [63] J. M. Tomczak, M. Casula, T. Miyake, S. Biermann, **Asymmetry in band widening and quasiparticle lifetimes in srvo₃: Competition between screened exchange and local correlations from combined gw and dynamical mean-field theory gw + DMFT**, Phys. Rev. B 90 (2014) 165138. doi:10.1103/PhysRevB.90.165138.
URL <http://link.aps.org/doi/10.1103/PhysRevB.90.165138>
- [64] T. Miyake, C. Martins, R. Sakuma, F. Aryasetiawan, **Effects of momentum-dependent self-energy in the electronic structure of correlated materials**, Phys. Rev. B 87 (2013) 115110. doi:10.1103/PhysRevB.87.115110.
URL <http://link.aps.org/doi/10.1103/PhysRevB.87.115110>
- [65] L. Boehnke, F. Nilsson, F. Aryasetiawan, P. Werner, **When strong correlations become weak: Consistent merging of gw and dmft**, Phys. Rev. B 94 (2016) 201106. doi:10.1103/PhysRevB.94.201106.
URL <http://link.aps.org/doi/10.1103/PhysRevB.94.201106>
- [66] J. A. Moyer, C. Eaton, R. Engel-Herbert, **Highly conductive srvo₃ as a bottom electrode for functional perovskite oxides**, Advanced Materials 25 (26) (2013) 3578–3582. doi:10.1002/adma.201300900.
URL <http://dx.doi.org/10.1002/adma.201300900>
- [67] Z. Zhong, M. Wallerberger, J. M. Tomczak, C. Taranto, N. Parragh, A. Toschi, G. Sangiovanni, K. Held, **Electronics with correlated oxides: srvo₃/srto₃ as a mott transistor**, Phys. Rev. Lett. 114 (2015) 246401. doi:10.1103/PhysRevLett.114.246401.
URL <http://link.aps.org/doi/10.1103/PhysRevLett.114.246401>
- [68] L. Zhang, Y. Zhou, L. Guo, W. Zhao, A. Barnes, H.-T. Zhang, C. Eaton, Y. Zheng, M. Brahlek, H. F. Haneef, N. J. Podraza, M. H. W. Chan, V. Gopalan, K. M. Rabe, R. Engel-Herbert, **Correlated metals as transparent conductors**, Nat Mater 15 (2) (2016) 204–210, article.
URL <http://dx.doi.org/10.1038/nmat4493>
- [69] J. M. Tomczak, M. van Schilfgaarde, G. Kotliar, **Many-body effects in iron pnictides and chalcogenides: Nonlocal versus dynamic origin of effective masses**, Phys. Rev. Lett. 109 (2012) 237010. doi:10.1103/PhysRevLett.109.237010.
URL <http://link.aps.org/doi/10.1103/PhysRevLett.109.237010>
- [70] T. Schäfer, A. Toschi, J. M. Tomczak, **Separability of dynamical and nonlocal correlations in three dimensions**, Phys. Rev. B 91 (2015) 121107. doi:10.1103/PhysRevB.91.121107.
URL <http://link.aps.org/doi/10.1103/PhysRevB.91.121107>
- [71] Y. Lan, X. Chen, M. He, **Structure, magnetic susceptibility and resistivity properties of srvo₃**, Journal of Alloys and Compounds 354 (1) (2003) 95 – 98. doi:https://doi.org/10.1016/S0925-8388(02)01349-X.
URL <http://www.sciencedirect.com/science/article/pii/S092583880201349X>
- [72] E. Burzo, **5.1.4.2 magnetization and magnetic susceptibilities: Datasheet from landolt-börnstein - group iii condensed matter · volume 27f1α: “perovskites i (part a)” in springermaterials** (http://dx.doi.org/10.1007/10037300_17), copyright 1996 Springer-Verlag Berlin Heidelberg. doi:10.1007/10037300_17.
URL http://materials.springer.com/lb/docs/sm_lbs_978-3-540-46420-4_17